Hindawi
International Journal of Antennas and Propagation
Volume 2019, Article ID 1645281, 12 pages
https://doi.org/10.1155/2019/1645281

Research Article

Design and Implementation of Single-Layer 4×4 and 8×8 Butler Matrices for Multibeam Antenna Arrays

George A. Adamidis,[1] Ioannis O. Vardiambasis,[1] Melina P. Ioannidou,[2] and Theodoros N. Kapetanakis[1]

[1]*Department of Electronic Engineering, Faculty of Applied Sciences, Technological Educational Institute (TEI) of Crete, GR-73133 Chania, Crete, Greece*
[2]*Department of Electronic Engineering, Alexander Technological Educational Institute of Thessaloniki, GR-57400 Thessaloniki, Greece*

Correspondence should be addressed to Ioannis O. Vardiambasis; ivardia@chania.teicrete.gr

Received 29 September 2018; Revised 23 December 2018; Accepted 10 January 2019; Published 31 March 2019

Academic Editor: Yu Jian Cheng

Single-layer 4 × 4 and 8 × 8 Butler matrices (BMs) that operate in the L and S bands are implemented in this paper. Easy-to-fabricate microstrip layout topologies are designed and constructed; the final arrangement of the BMs allows realization without any crossovers. The performance of the networks is evaluated by measuring their frequency response. The return loss (RL) and the isolation are below -15 dB over the operation bandwidth for all structures, whereas the average insertion loss is less than 1 dB for the 4 × 4 BM and does not exceed 3 dB for the 8 × 8 BM. The amplitude imbalance is at most 0.5 dB and 1.5 dB, for the 4 × 4 and the 8 × 8 BMs, respectively. Moreover, multibeam antenna arrays fed by the BMs are constructed. The radiation patterns are measured and compared with theoretical data; a good agreement is achieved. The side lobes are sufficiently low, compared to the theoretical predictions, whereas they are further reduced by applying appropriate excitation schemes to the input ports of the BMs.

1. Introduction

Switched-beam, also termed as multibeam, antennas draw strong interest nowadays; they may be implemented by using an antenna array fed by a beam-forming network (BFN) or, simply, beamformer. One of the most popular BFNs is the Butler matrix (BM) [1]. A typical BM is a passive, symmetric $N \times N$ network; N is usually a power of 2. Generally, the BM comprises couplers, phase shifters, and transmission lines. It possesses N input and N output ports; by exciting one input port at a time, the signal is divided equally into N output ports with different phases. A switched-beam antenna may be realized by connecting the output ports to the N elements of an antenna array [2].

The 4 × 4 BM is the most common structure; a variety of techniques and configurations have been presented in the literature for the realization of such a BM [3–13]. One of them is the CMOS technology, which has been used to implement a fully integrated 4 × 4 BM for smart antenna systems [3]. A design based on Lange couplers has been presented by [4] in an attempt to reduce the size of the structure with low cost. The size reduction of the network has, also, been achieved by using the substrate integrated waveguide (SIW) technology [5, 6]. Moreover, the glass-based thin film integrated passive device (TF-IPD) technology has been reported for designing a miniature BM without sacrificing the operation bandwidth [7], whereas a miniaturized BM network has been implemented by using stub-loaded transmission lines (STTLs) without loss of performance [8]. Recently, a vertically installed planar (VIP) structure has been proposed; it allows for a compact circuit size and a wide bandwidth [9]. A symmetric, single-layer topology has been adopted by [10] in order to produce flexible phase differences in the output ports, whereas a design based on the phase reconfigurable

synthesized transmission line (PRSTL) has been introduced for the realization of an extended 4×4 BM with 16 switchable beams [11]. An inherent problem in the design of a BM is the presence of crossovers, an issue that may be overcome by implementing a multilayer topology like the one applied by [5, 12, 13] in order to construct 4×4 BMs.

The design and implementation of an 8×8 BM may be a more challenging task because it is a more complicated network than the 4×4 BM and it involves more crossovers [14–22]. The dual-layer and the SIW technology have been adopted in order to decrease the complexity and reduce the size of a 4×8 BM [14], as well as an 8×8 BM [15]. A back--to-back, bilayer, microstrip configuration [16] and a three-layer configuration which incorporates one four-way differential phase shifter [17] have been applied in an attempt to avoid crossovers. Other realizations of 8×8 BMs involve lumped elements with a very small size [18], asymmetric couplers, and Wilkinson combiners in order to produce tapered amplitude distributions under standard single port excitation [19] and tunable phase shifters to provide full-beam switching/steering capability [20]. Furthermore, a fully planar design with two metallization layers and no interlayer connections has been proposed [21], whereas the appropriate connection of two pairs of identical 4×4 BMs has led to the development of an ultrabroadband 8×8 BM [22].

Single-layer BMs are designed, fabricated, and measured in this paper. Specifically, four different layouts are applied for the realization of four 4×4 BMs, respectively, whereas a layout of an 8×8 BM is presented. The main contribution of this paper is that although the topologies proposed are very low-cost, simple, and easy to fabricate, they exhibit attractive characteristics such as low insertion loss and small amplitude imbalance. All structures are realized by using a common FR4 laminate. Moreover, they avoid crossovers at the expense of having the input and output ports scattered around the network. As a result, full integration cannot be achieved between the BM and the antenna array; coaxial cable connections are required. The radiation characteristics of a multibeam antenna fed by the developed BMs are calculated and measured by constructing two different types of antenna arrays and connecting their elements to the outputs of the BMs. Furthermore, the side lobe level (SLL) of the multibeam antenna is improved by exciting simultaneously specific pairs of the BMs' input ports.

This paper is organized as follows. Section 2 comprises a brief description of the 4×4 and 8×8 BMs. The various layouts proposed for the implementation of the BMs are presented in Section 3. Besides, the fabrication of the BMs is described therein. Representative measurements of the scattering (S-) parameters of the BMs are included in Section 4, together with pertinent discussion, assessment of the networks' performance, and comparisons with previous works. The realization of multibeam antenna arrays is described in Section 5. Furthermore, measurements of the radiation patterns are presented and compared to those derived theoretically. Section 6 addresses the implementation of a low-SLL multibeam antenna by choosing properly the excitation scheme of the BMs. Finally, Section 7 comprises the conclusions of this work.

2. Butler Matrix Analysis

A typical multibeam, uniform, linear antenna array consists of N, equally spaced, identical elements; they all have the same excitation amplitudes, but there is a (constant) difference in phase excitation between two adjacent elements [23]. Hereafter, β stands for the phase by which the current in each element leads the current of the preceding element, whereas d stands for the distance between two adjacent elements. In order to generate N independent beams, pointing at $\theta_i (i = 1, \ldots, N)$ and symmetrically located along the normal to the antenna aperture, a "classic" $N \times N$ BM may be realized in conjunction with, at least, N radiating elements.

The topologies of the 4×4 and 8×8 BMs implemented in this paper are presented in Figure 1. The 4×4 BM is enclosed by the dashed rectangle, and it constitutes part of the 8×8 BM. It comprises four 90° hybrid couplers and two -45° phase shifters. Ports $\underline{1}$-$\underline{4}$ serve as inputs, whereas ports $\underline{5}$-$\underline{8}$ serve as outputs; all ports of the 4×4 BM are underlined in order to distinguish them from the ports of the 8×8 BM. The latter employs twelve 90° hybrids and various phase shifters as shown in Figure 1. It comprises 8 inputs (ports 1-8) and 8 outputs (ports 9-16); 8 independent, orthogonal beams may be generated by connecting the outputs to an 8-element antenna array and by exciting one input port at a time.

The phase progressions may be derived from $\beta_i = \pm(1 + 2m)(180^\circ/N)$, $i = 1, \ldots, N$, and $m = 0, 1, \ldots, (N/2) - 1$ [24]; they are summarized in Tables 1 and 2, for the 4×4 and 8×8 BM, respectively. Moreover, the phase at each output port is given therein. The beam directions are listed in the last column of Tables 1 and 2. They are calculated from $\theta_i = \cos^{-1}(\beta_i/kd)$, where $k = 2\pi/\lambda$ is the propagation constant in free space and λ stands for the wavelength; a half-wavelength distance has been assumed between two adjacent elements of the antenna array, i.e., $d = \lambda/2$.

3. Design and Fabrication of the BMs

Four different microstrip layout topologies have been applied in order to implement the 4×4 BM, and they are shown under scale in Figure 2, whereas the layout of the 8×8 BM is presented in Figure 3. The phase shifters are actually microstrip lines with a fixed length; some of them are marked in Figure 3 together with their length. All ports are isolated from each other, and they are matched to the fixed impedance 50Ω. The corresponding width of the microstrip lines is given in Figure 3.

As regards the 4×4 BM, the aim of designing several layouts has been the minimization of losses and the maximization of the bandwidth. Their main differences lie in the total length of the microstrip lines, the arrangement of the ports around the network, and the shape of the 90° hybrid couplers. Three different shapes have been employed and tested for the couplers: diamonds (Figure 2(a)), rectangles (Figures 2(b) and 2(d)), and circles (Figure 2(c)), with the latter possessing the smoothest bends and the shortest path. All designs are simple and easy to fabricate; the layout of Figure 2(b) has the smallest size, whereas that of

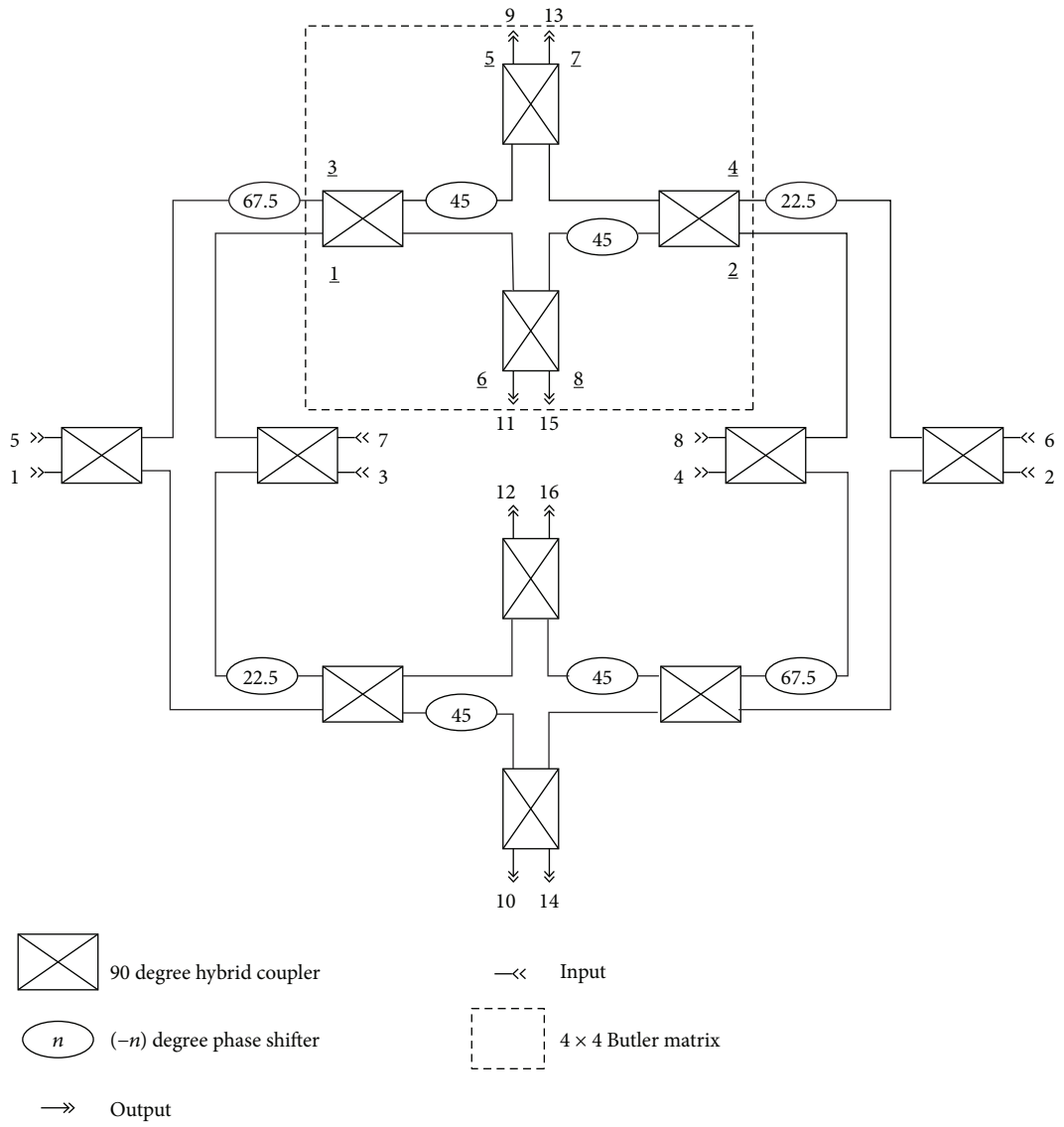

Figure 1: Topologies of the 4×4 and the 8×8 BMs.

Table 1: Output phases, phase progressions (β_i), and beam directions (θ_i) of the 4×4 BM.

Input port/beam	Output phase (deg) Port 5	Port 6	Port 7	Port 8	β_i (deg)	θ_i (deg)
1	45	-180	-45	90	135	41.4
2	0	45	90	135	45	75.5
3	135	90	45	0	-45	104.5
4	90	-45	-180	45	-135	138.6

Figure 2(d) is similar, albeit with a different arrangement of ports. However, experimental tests have shown that all four layouts exhibit the same losses and bandwidth.

The design of the 4×4 BMs has been optimized for operation at 2.44 GHz, whereas the corresponding frequency for the 8×8 BM is 1.9 GHz; the ADS software has been used for the optimization of all designs.

The advantage of all layouts presented in Figures 2 and 3 is that they have been realized in a single layer, without any crossover section. As a result, certain ports of the 8×8 layout appear at the center of the structure, i.e., ports 3-4, 7-8, 11-12, and 15-16, whereas the rest are arranged in pairs along the four sides of the structure (Figure 3). Experimental tests have shown that losses are minimized if the connectors are all mounted from the ground plane side, despite the position of the corresponding port. 4-hole flange mount jack receptacle SMA connectors have been used; the 4-hole mount flange of each connector was soldered on the ground plane, whereas the center sleeve of each connector was soldered directly on the corresponding microstrip line as shown in Figure 4.

A very low-cost laminate has been adopted to construct the BMs; they have been fabricated on an FR4 substrate with thickness of 1.5 mm and measured relative dielectric permittivity and loss tangent $\varepsilon_r = 4.35$ and $\tan\delta = 0.01$, respectively. The fabricated prototypes of the 4×4 layouts that are depicted in Figures 2(b) and 2(c) are displayed in

Table 2: Output phases, phase progressions (β_i), and beam directions (θ_i) of the 8×8 BM.

Input port/beam	Output phase (deg)								β_i (deg)	θ_i (deg)
	Port 9	Port 10	Port 11	Port 12	Port 13	Port 14	Port 15	Port 16		
1	-112.5	45	-157.5	0	157.5	-45	112.5	-90	157.5	29
2	-112.5	0	112.5	-135	-22.5	90	-157.5	-45	112.5	51.3
3	-135	-67.5	0	67.5	135	-157.5	-90	-22.5	67.5	68
4	-180	-157.5	-135	-112.5	-90	-67.5	-45	-22.5	22.5	82.8
5	-22.5	-45	-67.5	-90	-112.5	-135	-157.5	-180	-22.5	97.2
6	-22.5	-90	-157.5	135	67.5	0	-67.5	-135	-67.5	112
7	-45	-157.5	90	-22.5	-135	112.5	0	-112.5	-112.5	128.7
8	-90	112.5	-45	157.5	0	-157.5	45	-112.5	-157.5	151

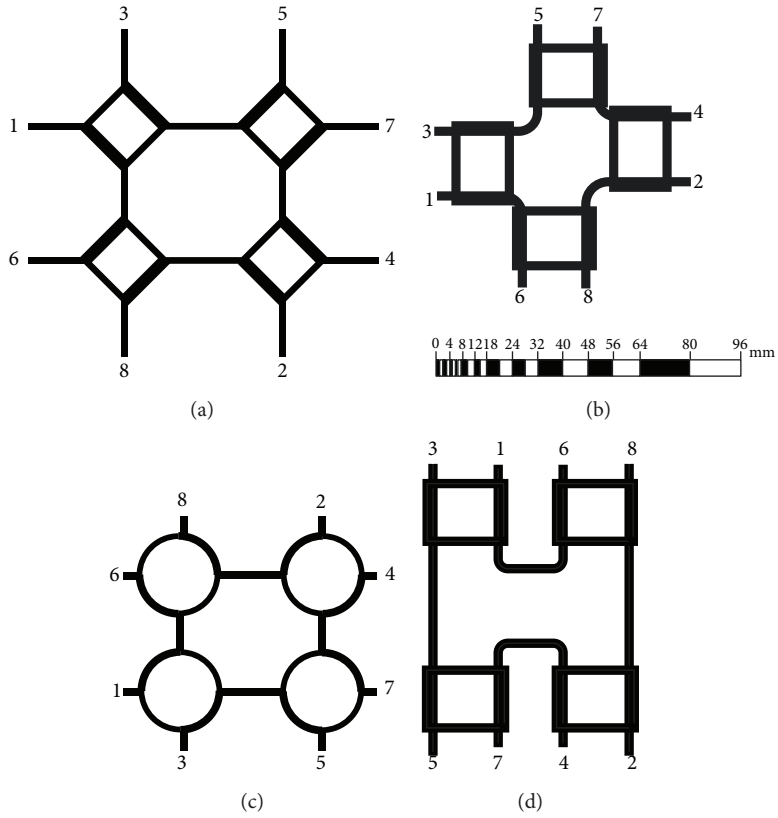

Figure 2: Four different layouts for the designed 4×4 BMs.

Figure 5(a) together with dimension tags, whereas the fabricated 8×8 BM is displayed in Figure 5(b). The corresponding pictures of the 4×4 BMs depicted in Figures 2(a) and 2(d) are omitted for the sake of brevity.

4. Measurements and Performance Evaluation of the Butler Matrices

The proposed BMs have been experimentally tested. As a first step, the S-parameters of all structures have been measured; since the entire set of measurements cannot be presented herein due to limited space, only indicative results are shown in Figures 6–9. Hereafter, all the results concerning the measured frequency response of the 4×4 BM refer to the structure of Figure 2(b) and are depicted in Figures 6 and 7, whereas Figures 8 and 9 refer to the 8×8 BM of Figure 3.

Figure 6(a) suggests that the measured $|S_{ii}|$, $i = 1, \ldots, 4$ are below -15 dB from 2.29 to 2.62 GHz (with the exception of $|S_{11}|$ which is slightly greater around 2.47 GHz), although the operation frequency is somewhat shifted mainly because of the fabrication tolerance. As regards the magnitude of the isolation coefficients between the input ports (Figure 6(b)), they are less than -15 dB over the 2.24-2.74 GHz bandwidth.

The measured magnitude response, when port 2 is fed, is plotted in Figure 7(a). Since the input signal is, eventually, distributed to four output ports with equal amplitudes the magnitude of the S-parameters depicted therein should approach the ideal value of -6 dB. The measured $|S_{i2}|$, $i = 5$,

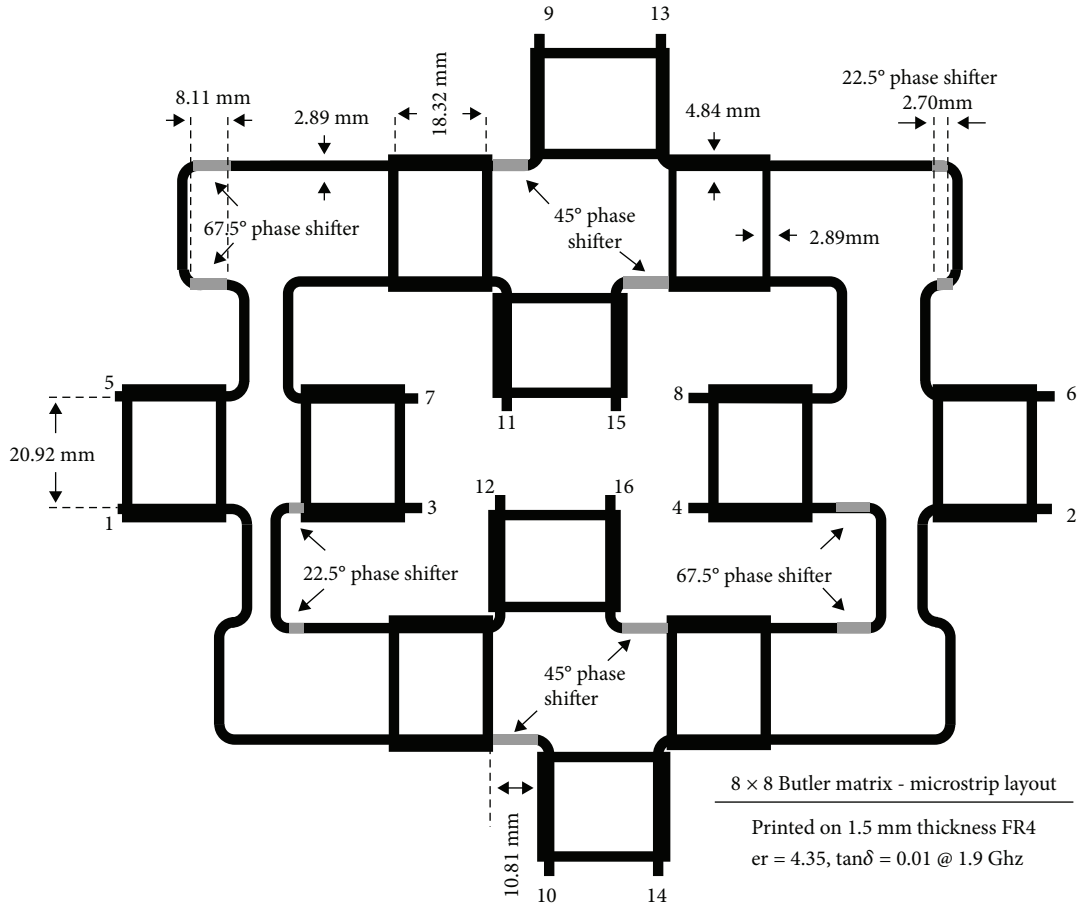

Figure 3: Layout of the designed 8×8 BM.

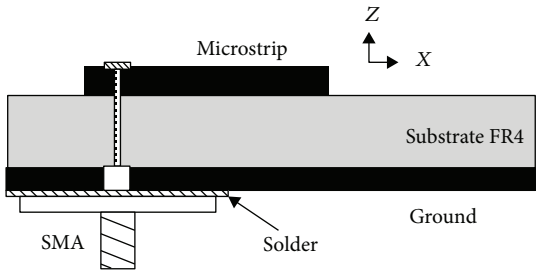

Figure 4: Cross-sectional view of the SMA connector soldering.

…, 8 are better than -7 dB over the range 2.32-2.52 GHz; other results (not reported herein for brevity) have shown that the amplitude imbalance of all the output signals, when different input ports are excited, does never exceed 0.5 dB in the aforementioned frequency range. Table 3 summarizes the performance of the BM presented herein and offers a comparison with other structures that operate in similar frequency bands. It may be verified that the proposed BM exhibits very low insertion losses and the smallest amplitude imbalance among similar structures. The transmission coefficients of the configurations reported in Table 3 are found in the range [-7.5, -11] dB, whereas the amplitude imbalance is not better than 1 dB.

Figure 7(b) demonstrates the measured phase differences $\angle S_{i+1,2} - \angle S_{i,2}$, $i = 5, 6, 7$. According to Table 1, these differences should be equal to $\beta_2 = 45°$. The curves of Figure 7(b) suggest that there is a good agreement between the measurements and the theoretical value, especially over the aforementioned 2.32-2.52 GHz bandwidth, where the phase difference deviation is ±3°. The same deviation has been observed for the phase differences $\angle S_{i+1,3} - \angle S_{i,3}$, i.e., $-45° \pm 3°$. The corresponding phase differences for beams 1 and 4, over 2.32-2.52 GHz, have been found $135° \pm 5°$ and $-135° \pm 7°$, respectively. Table 3 suggests that similar phase difference deviations may be found in the literature; it should be noted that the extremely low value achieved by [8] refers to the center frequency and not to the whole bandwidth of the BM.

As regards the 4×4 BMs depicted in Figures 2(a), 2(c), and 2(d), the measured S-parameters exhibit, more or less, the same behavior as the BM of Figure 2(b). Thus, the corresponding results are omitted to avoid redundancy.

The measured $|S_{ii}|$, $i = 1, \ldots, 8$, of the 8×8 BM developed herein are plotted in Figure 8(a). It may be verified that an RL better than -15 dB, for all the 8 inputs, is achieved from 1.8 to 2.03 GHz. As regards the outputs, the measured $|S_{ii}|$ for $i = 9, \ldots, 16$ (not shown herein) exhibit a similar behavior: they are all less than -15 dB over the range 1.8-2.07 GHz. Figure 8(b) illustrates the measured $|S_{i8}|$, $i = 1, \ldots, 7$; the isolation, between input ports when port 8 is fed, is better than

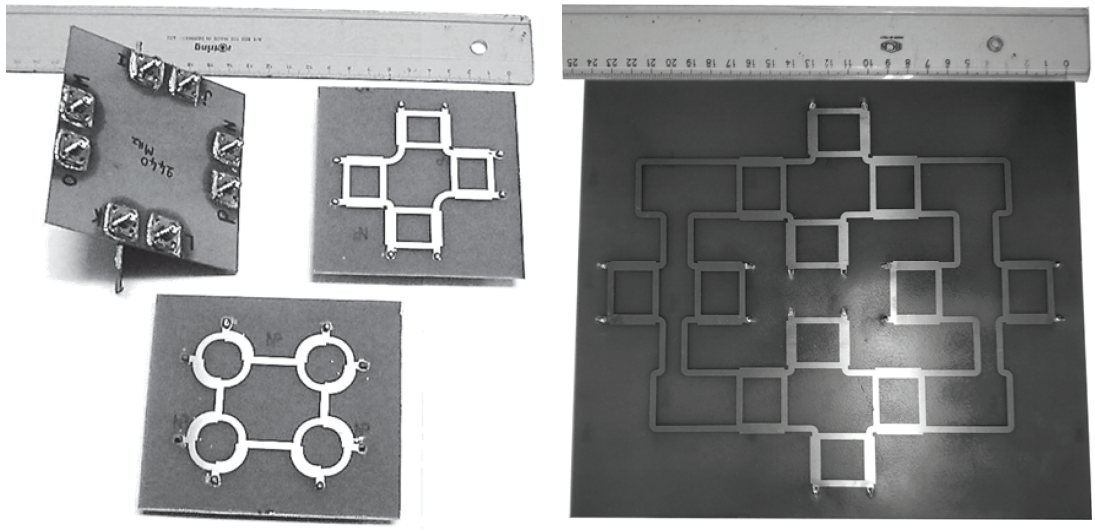

(a) (b)

Figure 5: Pictures of certain fabricated prototypes. (a) Top view of the 4×4 BMs that correspond to the layouts of Figures 2(b) and 2(c) and bottom view of the layout depicted in Figure 2(b). (b) Top view of the 8×8 BM.

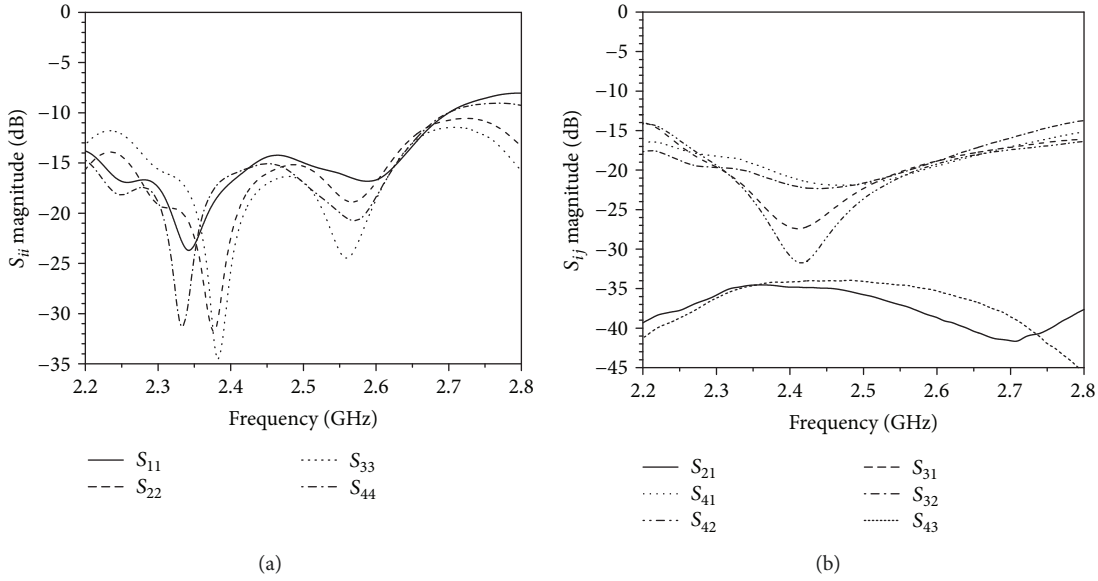

(a) (b)

Figure 6: Measured magnitude of (a) the return losses and (b) the isolation coefficients of the 4×4 BM.

15 dB in the range 1.78-2.18 GHz. According to the complete set of measurements (not presented herein), the narrowest frequency range, in order to keep the magnitude of the isolation coefficients below -15 dB, when any one of the input ports is excited, is 1.79-2.07 GHz.

The measured magnitudes of the S-parameters, when port 1 is fed, are presented in Figure 9(a). The ideal value for all curves plotted therein is -9 dB since the input signal is, eventually, distributed to 8 output ports with equal amplitudes. The measured $|S_{i1}|$, $i = 9, \ldots, 16$, are better than -12 dB over the 1.8-2.04 GHz bandwidth, with an average value of -11.7 dB. The insertion loss of 2.7 dB may be attributed to the dielectric losses which are more pronounced because of the relatively long paths among inputs and outputs. However, more important than $|S_{i1}|$ itself is the amplitude imbalance among the transmission coefficients. The maximum value of the amplitude imbalance, observed at 2.04 GHz, is 1.5 dB, whereas the mean amplitude imbalance in the aforementioned frequency range is 1 dB. Similar responses have been obtained for all the transmission coefficients. $|S_{i5}|$ exhibits the worst behavior with an average value of -12 dB over the range 1.8-2 GHz, whereas the best performance has been found for $|S_{i7}|$ with an average value of -11.3 dB over the range 1.78-2.04 GHz. The amplitude imbalance never exceeded 1.5 dB in the aforementioned bandwidths, whereas its mean value has been found equal to 1 (0.9) dB for $|S_{i5}|$ ($|S_{i7}|$). Results reported by other researchers are presented in the last three columns of

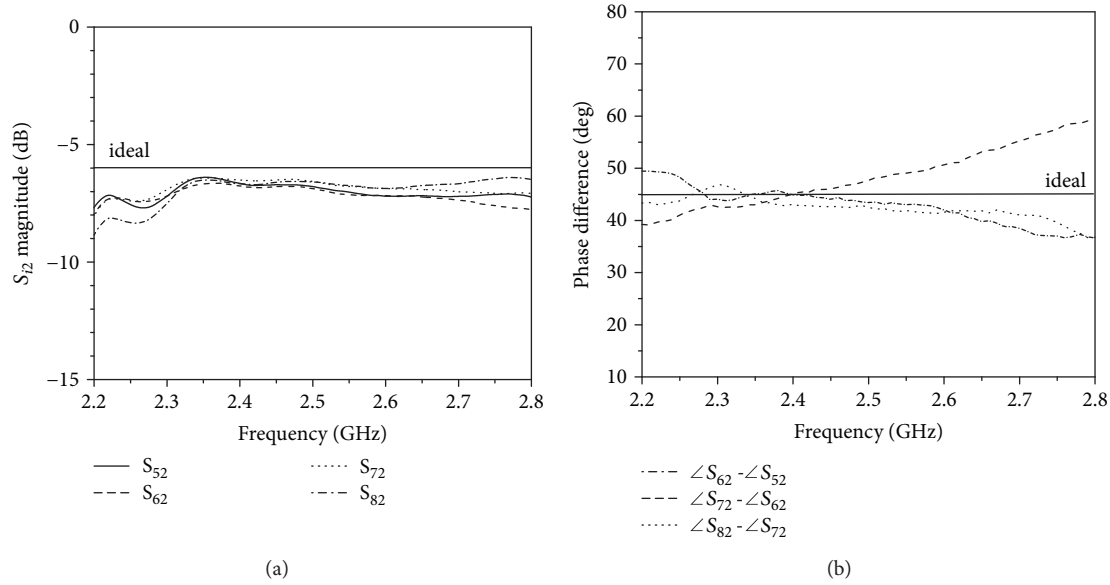

Figure 7: (a) Magnitude and (b) phase difference of the S-parameters for the 4×4 BM when input port 2 is excited.

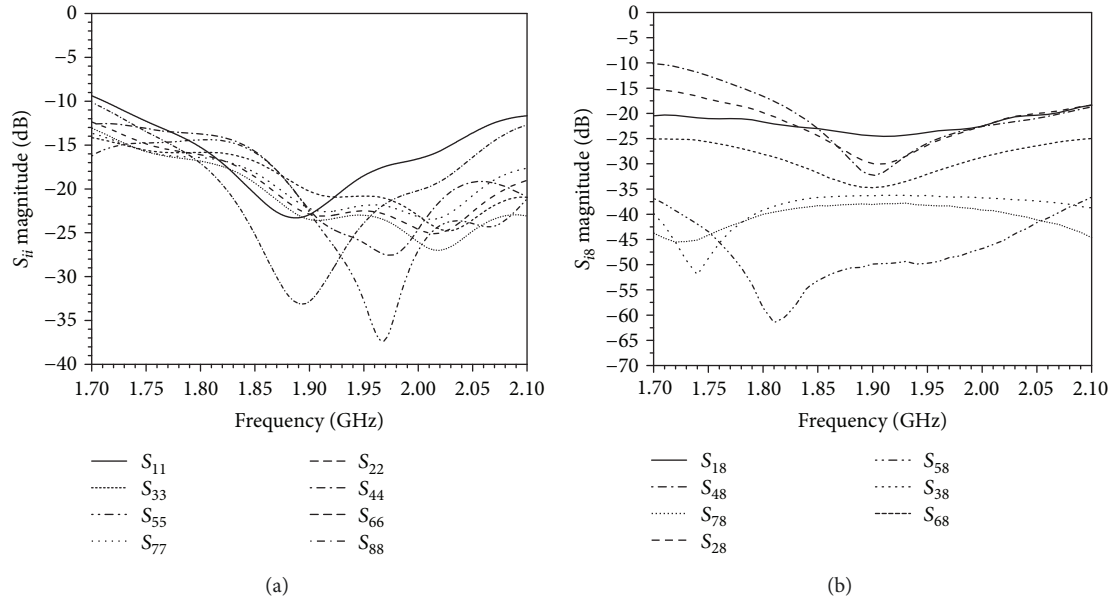

Figure 8: Measured (a) return loss and (b) isolation (magnitude) of the 8×8 BM.

Table 3. The insertion losses are all similar; i.e., the transmission coefficients are found in the range [-12.5, -11] dB, whereas the amplitude imbalance of this work, together with the one achieved by [24], is one of the smallest. However, the aforesaid comparisons may be used with cautiousness, since the 8×8 BMs presented in Table 3 do not operate in the same frequency bands.

The measured phase differences $\angle S_{i+1,1} - \angle S_{i,1}$, $i = 9, \ldots, 15$, are plotted in Figure 9(b). According to Table 2, these differences should be equal to $\beta_1 = 157.5^\circ$. A reasonable agreement is observed over the 1.8-2 GHz bandwidth, where the phase difference deviation is $\pm 12^\circ$. The phase differences for beams 2-7 have been measured $112.5^\circ \pm 10^\circ$, $67.5^\circ \pm 6^\circ$, $22.5^\circ \pm 7^\circ$, $-22.5^\circ \pm 8^\circ$, $-67.5^\circ \pm 9^\circ$, and $-112.5^\circ \pm 7^\circ$, respectively. The results for beam 8 have been excluded because of a system failure. It may be verified from Table 3 that the phase variation within the bandwidth of the proposed BM maintains a reasonable value compared to other configurations.

5. Multibeam Antenna Implementation

5.1. Construction of the Antenna Arrays. Four- and eight-element antenna arrays have been constructed and fed by the 4×4 and 8×8 BMs, respectively. Two types of vertically polarized antennas have been implemented: (a) an array of N printed dipoles of length $\lambda/2$ and (b) an array of N monopoles of length $\lambda/4$, where $N = 4$ (8) for the 4×4

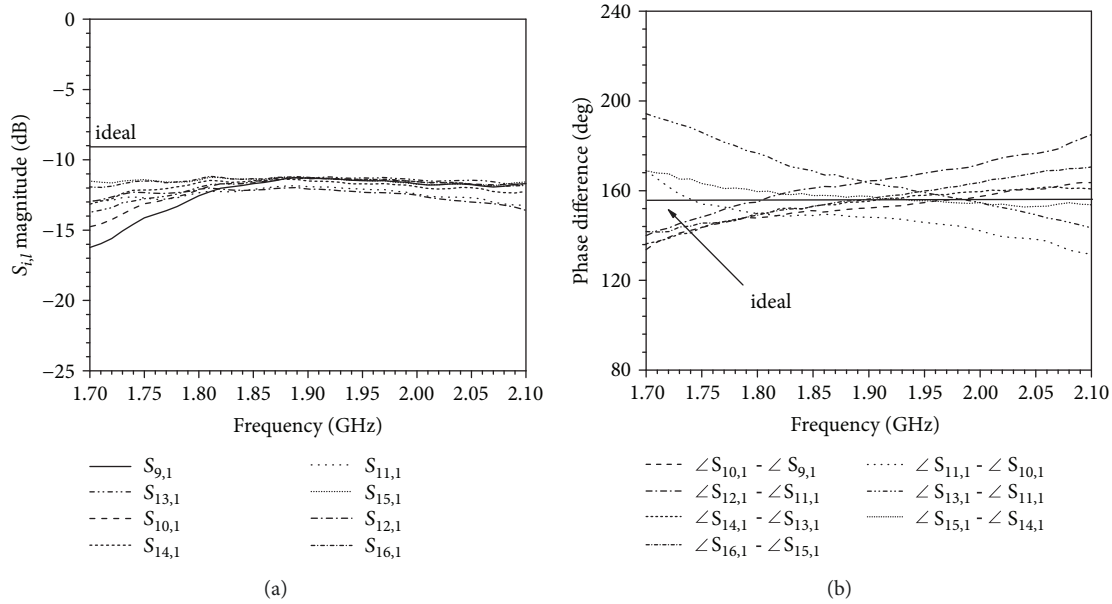

Figure 9: (a) Magnitude and (b) phase difference of the S-parameters for the 8×8 BM when input port 1 is excited.

(8×8) BM. The radiating elements have been placed in front of a plane reflector at a distance $a = 0.3\lambda$; their spacing has been $d = \lambda/2$.

The 8-element antenna arrays are depicted in Figure 10; the operating frequency has been taken equal to 1.9 GHz. As regards the 4-element arrays, they have been designed in a similar manner, albeit for the operating frequency of 2.44 GHz. The antenna array in this case comprises either 4 printed dipoles $\lambda/2$ or 4 monopoles $\lambda/4$ placed in front of a plane reflector. Figure 11 presents a picture of the complete configuration that comprises the 4×4 BM connected to the 4-monopole antenna array via coaxial cables of equal length. The input ports 1-4, the output ports 5-8, the array feeding cables, and the input from the RF generator to port 4 are clearly marked in Figure 11.

5.2. Radiation Patterns. The theoretical and measured radiation patterns of the structures developed in this paper are presented in Figures 12 and 13. The experimental results presented henceforth have been acquired by using the printed dipole antenna array with 4 or 8 elements. Besides, the measurements have been repeated with the 4- or 8-monopole antenna array in order to verify the experimental results. No discrepancies have been observed. The generated four beams of the 4-element antenna array, fed by the 4×4 BM of Figure 2(b), are normalized and depicted in Figure 12. It may be verified that the measured radiation patterns coincide, more or less, with the theoretical ones especially as regards the main lobes; the beams are successfully steered towards the directions predicted by theory (last column of Table 1). Figure 12 indicates that certain small discrepancies may occur between the theoretical and the measured results in the side lobes of the patterns. However, the measured SLLs never exceed -10 dB.

A comparison between the theoretical and measured radiation patterns of the 8-element antenna array, fed by the 8×8 BM of Figure 3, is offered by Figure 13. A rather good agreement is achieved between the measured and the theoretical results. The main lobe directions agree, more or less, with the theoretical predictions which are given in the last column of Table 2. The maximum error observed between the theoretical and the measured main lobe directions has been found equal to 3°, whereas the mean error, as derived from all experiments, is 2°. As regards the side lobes, the measurements may deviate from the theoretical results to a certain extent. However, the SLLs are less than -12 dB for all cases examined, which is a satisfactory outcome since the theoretical SLL value should approach the value of -13.2 dB for large N [25].

6. Side Lobe Level Reduction

The developed structures may be used to generate radiation patterns with significantly low side lobes, by exciting simultaneously multiple input ports of the BMs [2]. Specifically, if a pair of input ports is simultaneously excited, a cosine distribution is produced at the outputs; the SLL in this case is as low as -23 dB [19]. The aforementioned technique has been applied to the BMs developed herein, and the corresponding radiation patterns have been measured. The results given below refer to the 8-element antenna array fed by the 8×8 BM. Similar results have been produced for the 4-beam antenna and are omitted for brevity.

The linear combinations applied in order to excite the inputs of the 8×8 BM are listed in Table 4. Each row of the latter corresponds to a different excitation scheme indicating that a pair of adjacent input ports is excited at a time; the corresponding BM outputs are summarized in Table 5, together with the phase progressions. By connecting these outputs to the 8 elements of the antenna array, radiation patterns like the ones shown in Figure 14 are obtained.

Table 3: Comparison of the proposed BMs and previous works.

	This work	[3]	[7]	[8]	[13]	[9]	This work	[20]	[19]	[24]
Matrix order	4 × 4	4 × 4	4 × 4	4 × 4	4 × 4	4 × 4	8 × 8	8 × 8	8 × 8	8 × 8
Process	Single-layer PCB (FR4)	0.18 μm CMOS	Glass-based TF-IPD	Single-layer PCB (Rogers 5880)	Double-layer PCB (FR4)	VIP	Single-layer PCB (FR4)	Multilayer PCB	Single-layer PCB (Rogers 4003C)	PCB-Integrated stripline
Bandwidth (GHz)	2.32-2.52	2.4-2.6	2.4-2.6	2.2-2.6	2.4**	1.3-2.32	1.8-2	1.6-2.8	2.4-2.5	2.5-3.5
Input RL* (dB)	-15	-20	-13	-10	-10**	-10	-15	–	-13	-20
Transmission coef.* (dB)	-7	-11	-10	-8.2	-10**	-7.5	-12	-11.6	-12.5	-11
Amplitude imbalance* (dB)	0.5	1.5	1.1	1.7	3**	±1	1.5	±1.5	±1	±0.5
Phase error* (deg)	±7	±4	±13	±2.1**	±7**	±7	±12	±31	±12.5	±10

*Within the whole BW, worst case. **Refers to the center frequency.

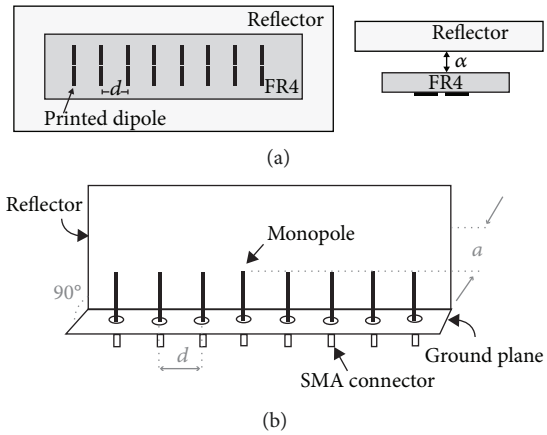

Figure 10: (a) The 8-printed dipole (the FR4 is 59.4×6.4 and the reflector 59.4×21) and (b) the 8-monopole (the ground plane is 59.4×8.9 and the reflector is 59.4×21) antenna array. The dimensions are given in cm.

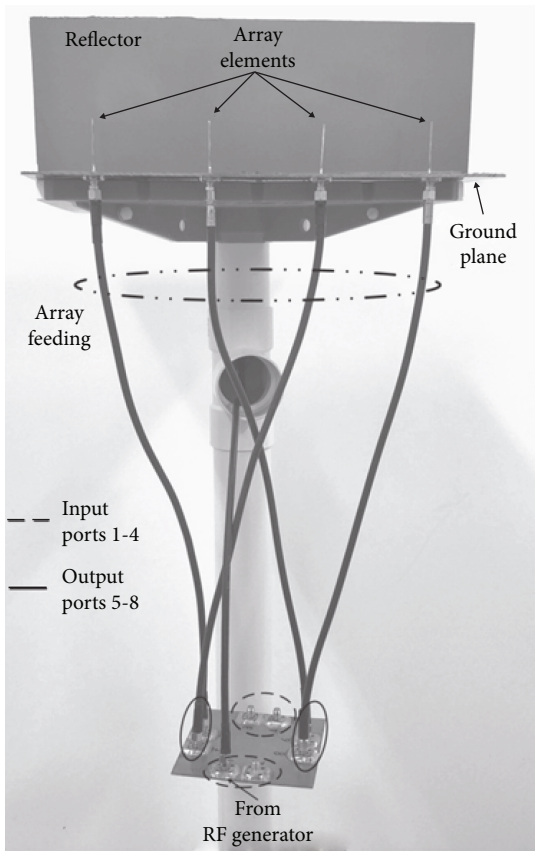

Figure 11: Picture of the 4×4 BM connected to the 4-monopole antenna.

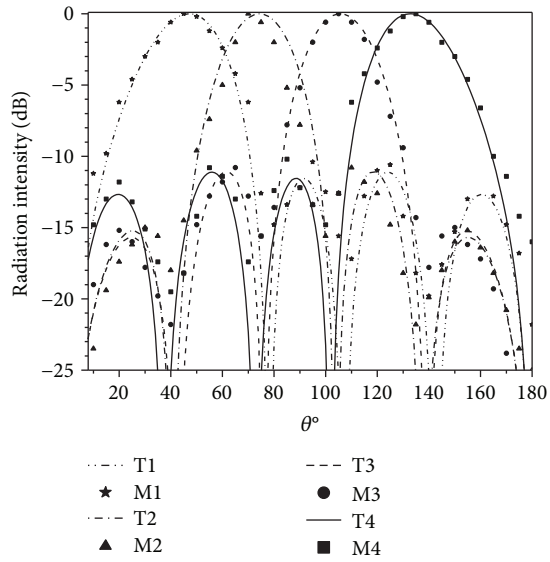

Figure 12: Normalized radiation patterns at 2.44 GHz of the 4-element antenna array fed by the 4×4 BM shown in Figure 2(b). The curves T1-T4 depict the theoretical results that correspond to beams 1-4, respectively, of Table 1. Accordingly, M1-M4 stand for the measurements.

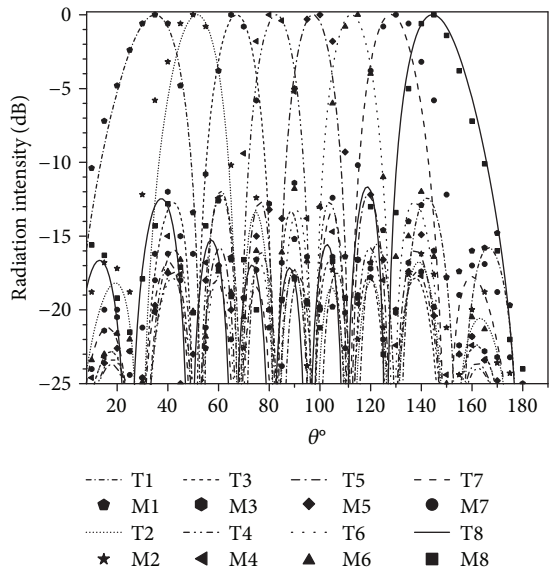

Figure 13: Normalized radiation patterns at 1.9 GHz of the 8-element antenna array fed by the 8×8 BM. The curves T1-T8 depict the theoretical results that correspond to beams 1-8, respectively, of Table 2. Accordingly, M1-M8 stand for the measurements.

On the one hand, the measured main lobes have a good performance when compared to the theoretical results. Figure 14 suggests that the shift of the maximum beam direction is rather negligible; the same remark holds for all beams listed in Tables 3 and 4, but the corresponding results are omitted for brevity. On the other hand, certain discrepancies may be observed between the theoretical and the measured side lobes. However, the SLL has been found below -20 dB, for all cases examined, which is a rather satisfactory result compared to the theoretical value of -23 dB. Moreover, the measured SLLs constitute a considerable improvement over the value of -12 dB obtained with uniform amplitude excitation of the BM (Section 5).

Table 4: Inputs of the 8×8 BM in order to produce the radiation patterns of Figure 14. ($\varphi_1 = -202.5^\circ$, $\varphi_2 = -157.5^\circ$).

Beam	Input							
	Port 1	Port 2	Port 3	Port 4	Port 5	Port 6	Port 7	Port 8
A	0	0	0	1	1	0	0	0
B	0	1	-1	0	0	0	0	0
C	0	0	0	0	0	-1	1	0
D	1	$1\angle\varphi_1$	0	0	0	0	0	0
E	0	0	0	0	$1\angle\varphi_2$	1	0	0
F	0	0	1	$1\angle\varphi_2$	0	0	0	0
G	0	0	0	0	0	0	$1\angle\varphi_1$	1

Table 5: Outputs and phase progressions (β_i) of the 8×8 BM for the excitation shown in Table 4.

Beam	Port 9	Port 10	Port 11	Port 12	Port 13	Port 14	Port 15	Port 16	β_i (deg)
	Output phase (deg)								
A	0	0	0	0	0	0	0	0	0
B	-123.75	146.25	56.25	-33.75	-123.75	146.25	56.25	-33.75	90
C	-33.75	56.25	146.25	-123.75	-33.75	56.25	146.25	-123.75	-90
D	-33.75	101.25	-123.75	11.25	146.65	-78.75	56.25	-168.75	135
E	-101.25	-146.25	168.75	-123.75	78.75	33.75	-11.25	-56.25	-45
F	-56.25	-11.25	33.75	78.75	-123.75	168.75	-146.25	-101.25	45
G	-168.75	56.25	-78.75	146.65	11.25	-123.75	-146.25	-33.75	-135
	Output amplitude (relative)								
A-G	0.138	0.393	0.588	0.693	0.693	0.588	0.393	0.138	

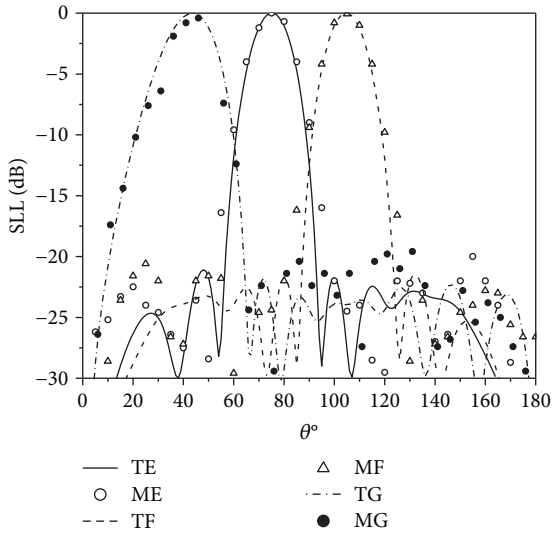

Figure 14: Normalized radiation patterns at 1.9 GHz of the 8-element antenna array fed by the 8×8 BM, according to the schemes shown in the last 3 rows of Table 4. The curves TE, TF, and TG depict the theoretical results that correspond to beams E, F, and G, respectively. Accordingly, ME, MF, and MG stand for the measurements.

7. Conclusions

Simple and inexpensive 4×4 and 8×8 BMs, at 2.44 and 1.9 GHz, respectively, have been designed and fabricated in this paper. All networks have been implemented in a single layer, without any crossovers. Four different layouts have been developed for the 4×4 BM; all of them have been proven to possess very similar characteristics. The actual bandwidth of the networks has been determined by measuring their *S*-parameters. As regards the 4×4 BMs, operation in the range 2.32-2.52 GHz may guarantee that the return losses and the isolation coefficients are kept below -15 dB for all ports, whereas the transmission coefficients are all better than -7 dB with an amplitude imbalance less than 0.5 dB. The corresponding bandwidth for the 8×8 BM is 1.8-2 GHz; it has been obtained by enforcing the limits of -15 dB for the return losses and the isolation coefficients and -12 dB for the transmission coefficients; the average amplitude imbalance of the latter is 1 dB. The deviations of the phase difference between two adjacent output ports do not exceed $\pm 7^\circ (\pm 12^\circ)$ for the $4 \times 4 (8 \times 8)$ BMs in the aforementioned frequency ranges.

Four- and 8-element antenna arrays have been constructed and connected to the outputs of the BMs in order to test the radiation characteristics of the resulting multibeam antennas. The radiation patterns of all structures have been measured. The experimental results have been compared to the theoretical predictions, and a good agreement has been observed. An average deviation of 2° between the measured and the theoretical maximum beam direction has been obtained, whereas the SLLs have never exceeded -10 dB and -12 dB for the 4×4 and 8×8 BMs, respectively.

Furthermore, the side lobes have been successfully reduced to at least -20 dB by exciting simultaneously two adjacent input ports of the BMs.

Data Availability

All experiments were part of the activities of the Laboratory of Telecommunications and Electromagnetic Applications of the Technological Educational Institute of Crete, and the corresponding data are available upon request.

Conflicts of Interest

The authors declare that that there is no conflict of interest regarding the publication of this paper.

References

[1] J. Butler and R. Lowe, "Beamforming matrix simplifies design of electronically scanned antennas," *Electron Design*, vol. 9, pp. 170–173, 1961.

[2] A. K. Bhattacharyya, *Phased Array Antennas; Floquet Analysis, Synthesis, BFNs, and Active Array Systems*, Wiley, 2006.

[3] C.-C. Chang, T.-Y. Chin, J.-C. Wu, and S.-F. Chang, "Novel design of a 2.5-GHz fully integrated CMOS Butler matrix for smart-antenna systems," *IEEE Transactions on Microwave Theory and Techniques*, vol. 56, no. 8, pp. 1757–1763, 2008.

[4] M. Traii, M. Nedil, A. Gharsallah, and T. A. Denidni, "A new design of compact 4×4 Butler matrix for ISM applications," *International Journal of Microwave Science and Technology*, vol. 2008, Article ID 784526, 7 pages, 2008.

[5] A. A. M. Ali, N. J. G. Fonseca, F. Coccetti, and H. Aubert, "Design and implementation of two-layer compact wideband Butler matrices in SIW technology for Ku-band applications," *IEEE Transactions on Antennas and Propagation*, vol. 59, no. 2, pp. 503–512, 2011.

[6] S. Karamzadeh, V. Rafii, M. Kartal, and B. S. Virdee, "Compact and broadband 4×4 SIW Butler matrix with phase and magnitude error reduction," *IEEE Microwave and Wireless Components Letters*, vol. 25, no. 12, pp. 772–774, 2015.

[7] Y. S. Lin and J. H. Lee, "Miniature Butler matrix design using glass-based thin-film integrated passive device technology for 2.5-GHz applications," *IEEE Transactions on Microwave Theory and Techniques*, vol. 61, no. 7, pp. 2594–2602, 2013.

[8] W. Nie, Y. Fan, S. Luo, and Y. Guo, "A switched-beam microstrip antenna array with miniaturized Butler matrix network," *Microwave and Optical Technology Letters*, vol. 57, no. 4, pp. 841–845, 2015.

[9] Q. P. Chen, Z. Qamar, S. Y. Zheng, Y. Long, and D. Ho, "Design of a compact wideband Butler matrix using vertically installed planar structure," *IEEE Transactions on Components, Packaging and Manufacturing Technology*, vol. 8, no. 8, pp. 1420–1430, 2018.

[10] H. Ren, B. Arigong, M. Zhou, J. Ding, and H. Zhang, "A novel design of 4×4 Butler matrix with relatively flexible phase differences," *IEEE Antennas and Wireless Propagation Letters*, vol. 15, pp. 1277–1280, 2016.

[11] H. N. Chu and T. G. Ma, "An extended 4×4 Butler matrix with enhanced beam controllability and widened spatial coverage," *IEEE Transactions on Microwave Theory and Techniques*, vol. 66, no. 3, pp. 1301–1311, 2018.

[12] M. Traii, M. Nedil, A. Gharsallah, and T. A. Denidni, "A novel wideband Butler matrix using multilayer technology," *Microwave and Optical Technology Letters*, vol. 51, no. 3, pp. 659–663, 2009.

[13] S. F. Ausordin, S. K. A. Rahim, N. Seman, R. Dewan, and B. M. Sa'ad, "A compact 4×4 butler matrix on double-layer substrate," *Microwave and Optical Technology Letters*, vol. 56, no. 1, pp. 223–229, 2014.

[14] J. W. Lian, Y. L. Ban, C. Xiao, and Z. F. Yu, "Compact substrate-integrated 4×8 Butler matrix with sidelobe suppression for millimeter-wave multibeam application," *IEEE Antennas and Wireless Propagation Letters*, vol. 17, no. 5, pp. 928–932, 2018.

[15] L. H. Zhong, Y. L. Ban, J. W. Lian, Q. L. Yang, J. Guo, and Z. F. Yu, "Miniaturized SIW multibeam antenna array fed by dual-layer 8×8 Butler matrix," *IEEE Antennas and Wireless Propagation Letters*, vol. 16, pp. 3018–3021, 2017.

[16] Y. Zhai, X. Fang, K. Ding, and F. He, "Miniaturization design for 8×8 Butler matrix based on back-to-back bilayer microstrip," *International Journal of Antennas and Propagation*, vol. 2014, Article ID 583903, 7 pages, 2014.

[17] H. L. Ting, S. K. Hsu, and T. L. Wu, "Broadband eight-port forward wave directional couplers and four-way differential phase shifter," *IEEE Transactions on Microwave Theory and Techniques*, vol. 66, no. 5, pp. 2161–2169, 2018.

[18] B. Cetinoneri, Y. A. Atesal, and G. M. Rebeiz, "An 8×8 Butler matrix in 0.13 -μm CMOS for 5-6GHz multibeam applications," *IEEE Transactions on Microwave Theory and Techniques*, vol. 59, no. 2, pp. 295–301, 2011.

[19] F. E. Fakoukakis, T. N. Kaifas, E. E. Vafiadis, and G. A. Kyriacou, "Design and implementation of Butler matrix-based beam-forming networks for low sidelobe level electronically scanned arrays," *International Journal of Microwave and Wireless Technologies*, vol. 7, no. 1, pp. 69–79, 2015.

[20] C.-C. Chang, R.-H. Lee, and T.-Y. Shih, "Design of a beam switching/steering Butler matrix for phased array system," *IEEE Transactions on Antennas and Propagation*, vol. 58, no. 2, pp. 367–374, 2010.

[21] K. Wincza, S. Gruszczynski, and K. Sachse, "Broadband planar fully integrated 8×8 Butler matrix using coupled-line directional couplers," *IEEE Transactions on Microwave Theory and Techniques*, vol. 59, no. 10, pp. 2441–2446, 2011.

[22] K. Wincza, S. Gruszczynski, K. Sachse, and S. Kuta, "Ultra-broadband 8×8 Butler matrix designed with the use of multi-sectional directional couplers and phase correction networks," *Microwave and Optical Technology Letters*, vol. 54, no. 6, pp. 1375–1380, 2012.

[23] C. A. Balanis, *Antenna Theory Analysis and Design*, Wiley, 2nd edition, 1997.

[24] K. Wincza and S. Gruszczynski, "Broadband integrated 8×8 Butler matrix utilizing quadrature couplers and Schiffman phase shifters for multibeam antennas with broadside beam," *IEEE Transactions on Microwave Theory and Techniques*, vol. 64, no. 8, pp. 2596–2604, 2016.

[25] J. P. Shelton, "Reduced sidelobes for Butler-matrix-fed linear arrays," *IEEE Trans. Antennas Propag.*, vol. 17, no. 5, pp. 645–647, 1969.